Advances in Computational Design, *Vol. 11, No. 2 (2026) 145-169*
https://doi.org/10.12989/acd.2026.11.2.145

Techno-Press

Stress analysis and design optimization of double-layer tank bottoms

Haijun Deng[1], Lei Dong[1], Shuping Guo[1], Yong Yu[1], Fan Li[1], Shubing Zhao[2], Xinaer Mandaiye*[2]

[1]*Beijing Branch, China Petroleum Engineering Co., Ltd., CPE Building, No. 8 Xinxi Road, Haidian District, Beijing 100085, China*
[2]*Beijing Datong Rising Engineering Software Development Co., Ltd., No. 5-162, Huanke Middle Road, Jinqiao Science and Technology Industrial Base, Tongzhou Park, Zhongguancun Science and Technology Park Tongzhou District, Beijing 101113, China*

(Received June 24, 2025, Revised March 27, 2026, Accepted April 2, 2026)

Abstract. Bottom plate leakage is a critical failure mode in storage tank engineering, often causing environmental contamination and high remediation costs. To improve structural integrity and leak detection, double-layer steel bottom systems have been widely adopted and standardized in API 650 and EN 14015. This study evaluates five typical configurations (Structures A–E) using finite element analysis with both 2D and 3D models under hydrostatic loading. Structure D shows the most uniform stress distribution, while Structure E achieves minimal deformation with greater complexity. Parametric studies investigate the effect of rubber pad thickness and elastic modulus on stress and deformation, revealing limited influence on overall performance. A modulus-material mapping framework is established, correlating elastic modulus to commercially available elastomers such as EPDM, polyurethane, and HDPE. Polyurethane materials with elastic moduli between 10–50 MPa are identified as offering the best balance between mechanical performance and economic feasibility. This research provides theoretical and practical insights for optimizing double-layer tank bottom structures, supporting better material selection, safer designs, and more efficient long-term operation of liquid storage systems.

Keywords: cost-performance evaluation; double-layer tank bottom; elastomeric materials; finite element analysis; hydrostatic loading; rubber pad design; structural optimization

1. Introduction

With growing demands for safety, sustainability, and operational reliability in liquid storage and transport, the structural integrity of large storage tanks has become a major concern in both academia and industry. Among failure modes, bottom plate leakage is especially hazardous, often causing environmental contamination and costly remediation.

To mitigate this, double-layer steel bottom structures have been widely adopted and integrated into international standards such as API 650—Welded Tanks for Oil Storage, Appendix I, and EN 14015—Specification for Site-Built Vertical Steel Tanks, Appendix H [1, 2], offering enhanced load capacity and early leak detection.

*Corresponding author, M.Sc., E-mail: madensynar2@gmail.com

ISSN: 2383-8477 (Print), 2466-0523 (Online)

However, current standards primarily address geometric configuration and basic functionality, offering limited guidance on material selection or stiffness design—particularly for intermediate layers such as elastomeric pads. Field inspections indicate that poor stiffness compatibility at interfaces can lead to premature failure under settlement, thermal cycling, or dynamic loads, exposing a gap between design assumptions and real material behavior.

Recent studies have improved understanding of tank-bottom mechanics: [3] analyzed soil-structure interaction; Wang et al. [4] examined stress transfer due to bonding; Liu et al. [5] addressed corrosion-stress coupling. International efforts include fatigue evaluation under thermal loads [6] and composite reinforcement analysis [7].

Research on elastomeric materials has also expanded. Ohsaki et al. [8] and Lai et al. [9] modeled seismic behavior of rubber bearings; Nguyen et al. [10] used hyperelastic models in nonlinear FEA; Meghashree et al. [11] applied machine learning for performance prediction; and IRJAES [13] proposed simplified stiffness models. In monitoring, Zhang et al. [12] introduced digital twin systems; Kim et al. [14] developed embedded sensors; Hoang et al. [15]; and Lim and Lee [16] validated nonlinear material models; Shon et al. [17]

Nonetheless, the mechanical role of elastomeric interfaces in double-bottom tanks remains underexplored. Most research focuses on macro-level response, with limited attention to local stiffness, modulus effects, or real-material correspondence. Few studies link simulation parameters (e.g., modulus) to engineering-grade elastomers, limiting practical implementation.

This study conducts a nonlinear finite element analysis (FEA) of five representative double-bottom structures under hydrostatic loading, assessing how rubber pad thickness and modulus influence stress and deformation. A parametric model explores sensitivity ranges, and a modulus-material mapping is built using real elastomers (e.g., EPDM, PU, HDPE). A cost-performance evaluation framework supports material selection [18].

By integrating simulation, material mapping, and economic analysis, this study provides both theoretical insight and practical guidance for optimizing double-layer tank bottom design, contributing to safer and more efficient storage infrastructure under complex service conditions.

2. Finite element modeling and analysis method

2.1 Structural configurations of double-layer tank bottoms

The double-layer tank bottom structure is a composite system consisting of a primary (upper) and auxiliary (lower) bottom plate, designed to enhance load-bearing capacity, resist corrosion, and facilitate leak detection. This configuration is widely used in liquid storage tanks across petrochemical, energy, and environmental sectors. Five representative structural schemes—Structures A through E—are examined based on differing support and interface designs:

1) Structure A: External lower bottom plate with sand–concrete ring beam fill; no elastic foundation.

2) Structure B: Adds a rubber pad beneath the bottom plate to simulate flexible support.

3) Structure C: Uses an internal lower bottom plate with internal support pads between the steel layers.

4) Structure D: Builds on Structure C by replacing sand with fully filled concrete for improved rigidity and stress distribution.

5) Structure E: Incorporates a 3D I-beam steel frame for high stiffness and integrated leak detection space.

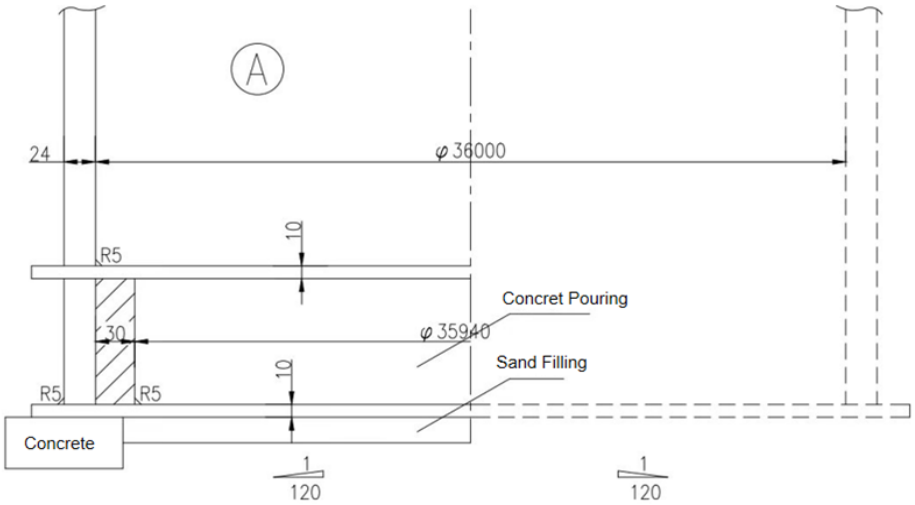

Figure 1. Finite element model of Structure A, featuring an external lower bottom plate with sand and a surrounding concrete ring beam; no elastic foundation is included (mm)

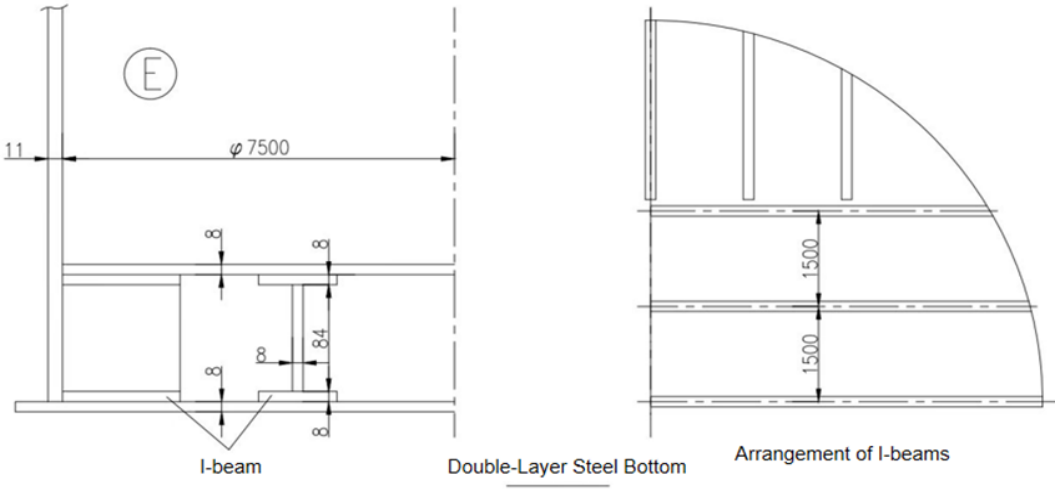

Figure 2. Finite element model of Structure E, supported by a steel I-beam grid system. The left panel shows the cross-sectional layout of the double-layer bottom, while the right panel illustrates the arrangement of I-beams for enhanced stiffness and integrated leak detection space (mm)

The configurations of Structure A and Structure E are shown in Figs. 1, 2, respectively, as representative examples.

Key components of the structure include double-layer bottom plates fillet-welded to the tank wall to form a sealed monitoring cavity; filler materials such as sand, concrete, or gravel, which help distribute stiffness and facilitate drainage; internal supports like steel pads or compacted filler to improve load transfer and reduce localized deformation; elastic interfaces in the form of rubber pads (as in Structure B) to simulate subgrade flexibility; and steel support systems, such as the I-beam frame in Structure E, that provide high localized bearing capacity.

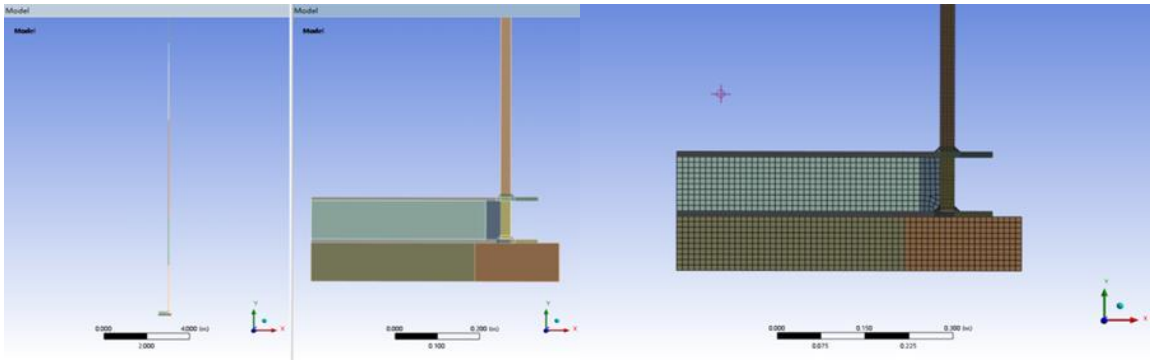

Figure 3. Finite Element Model of Structure A

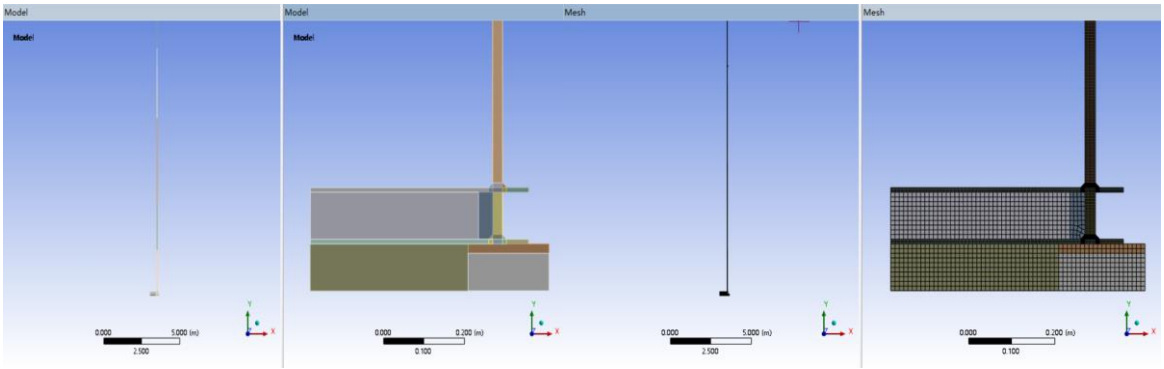

Figure 4. Finite Element Model of Structure B

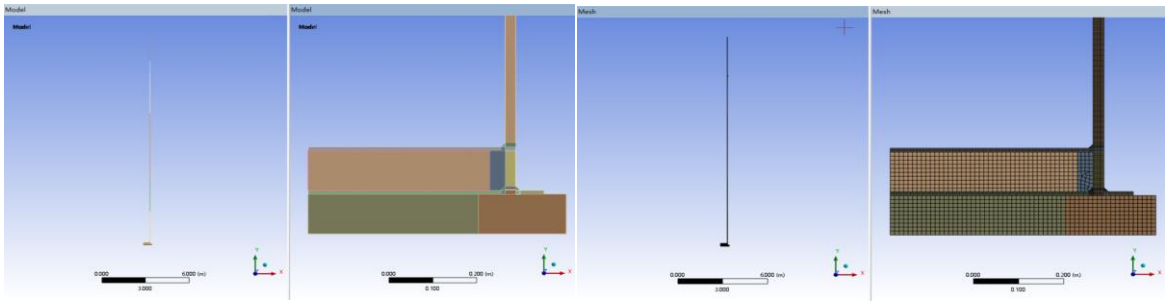

Figure 5. Finite Element Model of Structure C

2.2 Finite element analysis procedure

Finite element simulations are conducted using ANSYS software to analyze the mechanical behavior of the selected configurations under hydrostatic loading. The analysis focuses on quantifying stress concentration patterns, total deformation, and the effects of varying support conditions, especially in relation to elastomeric pads.

2.2.1 Geometric modeling in finite element analysis

Structures A–D are modeled using two-dimensional axisymmetric elements, appropriate for

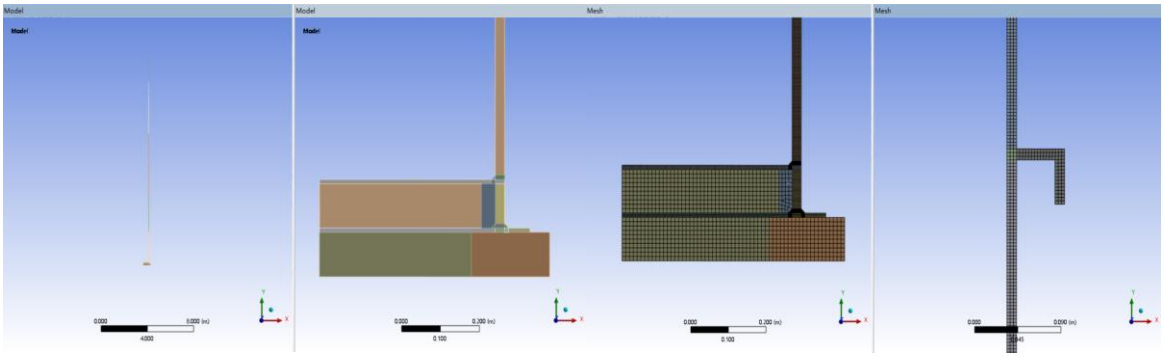

Figure 6. Finite Element Model of Structure D

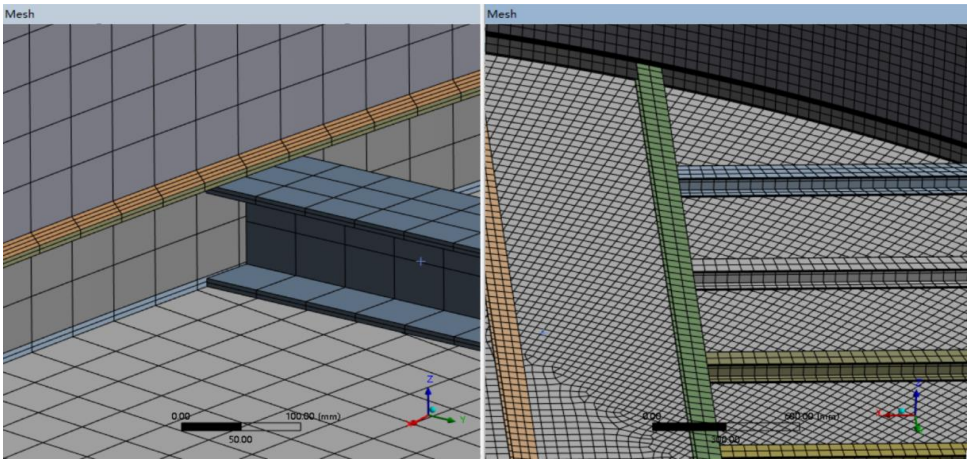

Figure 7. Finite Element Model of Structure E

tank configurations symmetric about the vertical axis. In contrast, Structure E employs a spatially asymmetric I-beam support layout and is therefore modeled as a full three-dimensional solid to accurately capture its load-bearing behavior [19].

To enhance engineering realism, the models incorporate key details such as fillet welds between bottom and wall plates, variable wall thickness, and inter-layer gaps. The corresponding geometries are shown in Fig. 3-7.

All structural models were developed from engineering drawings using the ANSYS finite element platform, ensuring consistency in geometry, material properties, and boundary conditions.

Structures A–D, exhibiting radial symmetry, use two-dimensional axisymmetric elements for computational efficiency and accurate global response. Structure E, featuring an asymmetric I-beam support system, is modeled with three-dimensional solid elements to capture localized stress effects.

Table 1 summarizes key design and modeling features of each configuration, including connection types, filler materials, internal supports, and analysis methods.

2.2.2 Structural feature summary

The major design features and finite element modeling strategies for each structural configuration are summarized in Table 1.

Table 1. Comparison of structural features of different tank bottom configurations

Structure ID	Connection Type of Second Bottom Plate	Filling Material	Internal Support Plate	Elastic Foundation	Model Type
A	External	Sand + Concrete Ring Beam	None	No	2D Axisymmetric
B	External	Sand + Concrete Ring Beam	None	Yes	2D Axisymmetric
C	Internal	Sand + Concrete Ring Beam	Yes	No	2D Axisymmetric
D	Internal	Fully Filled Concrete	Yes	No	2D Axisymmetric
E	Internal	I-Beam Support Structure	None	No	3D Solid Model

Table 2. Material properties used in simulation

Material	Density (kg/m³)	Elastic Modulus (MPa)	Poisson's Ratio	Yield Strength (MPa)	Allowable Stress (MPa)
A36 Steel	7850	2.0×10^5	0.3	250	120
Sand	1800	80	0.23	/	/
Concrete	2300	300	0.18	/	/
Rubber Pad (EPDM)	950	5.7	0.42	/	2.0 ~ 3.0
Material	Density (kg/m³)	Elastic Modulus (MPa)	Poisson's Ratio	Yield Strength (MPa)	Allowable Stress (MPa)

Note: In this study, the Poisson's ratio for rubber materials (e.g., EPDM) is set to 0.42. However, leading finite element platforms such as COMSOL and ANSYS recommend using Poisson's ratios in the range of 0.45 to 0.49 to better simulate the nearly incompressible behavior of rubber-like materials, as documented in their respective user manuals (COMSOL Multiphysics, n.d.; ANSYS Inc., n.d.). [30, 32]

2.2.3 Material properties

Materials are assigned based on typical engineering values. The metallic components are modeled as ASTM A36 steel (Standard Specification for Carbon Structural Steel, ASTM A36/A36M–14) [31], and non-metallic filler materials (sand, concrete, rubber) are assigned properties based on published mechanical data. Alternative binder systems such as BOFS-based geopolymers have also been investigated for durability and expansion control Onopriyenko et al. [36]. Material properties are listed in Table 2.

2.2.4 Meshing and convergence analysis

A mesh sensitivity analysis is performed using Structure B as a representative case. Element sizes are refined until changes in peak stress and deformation fall below 5%, ensuring a balance between computational efficiency and solution accuracy. Higher mesh densities are applied near fillet welds and interface transitions. The results are illustrated in Fig. 8.

2.2.5 Boundary conditions and loading

Boundary Conditions: The bottom surface of the structure is fixed to simulate a rigid subgrade. Symmetry boundary conditions are applied where applicable.

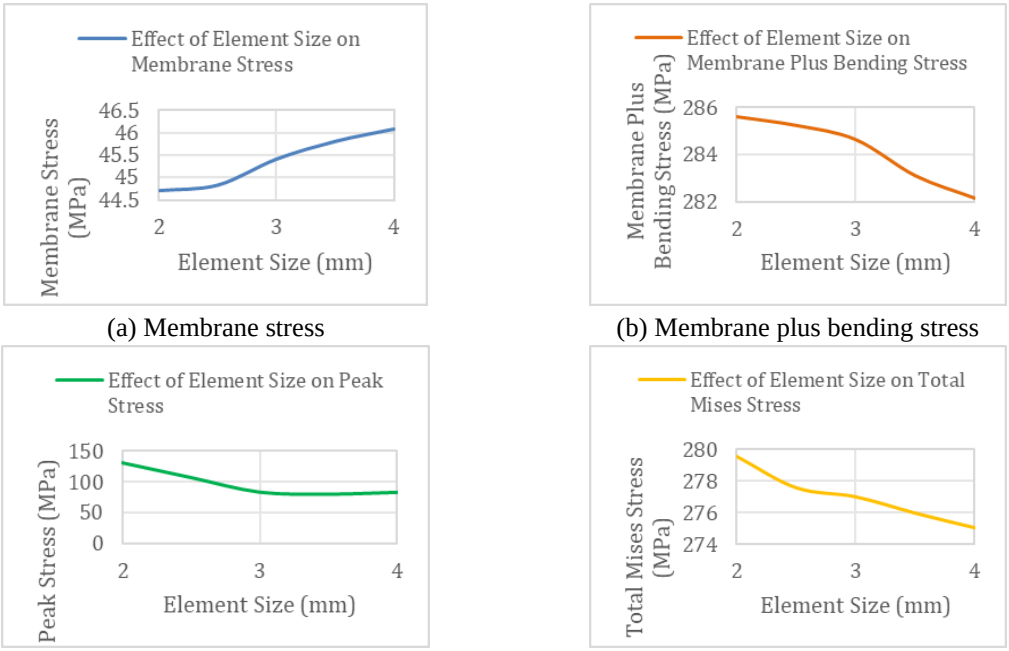

(a) Membrane stress (b) Membrane plus bending stress

(c) Peak stress (d) Total von Mises stress

Figure 8. Mesh Sensitivity Analysis Results

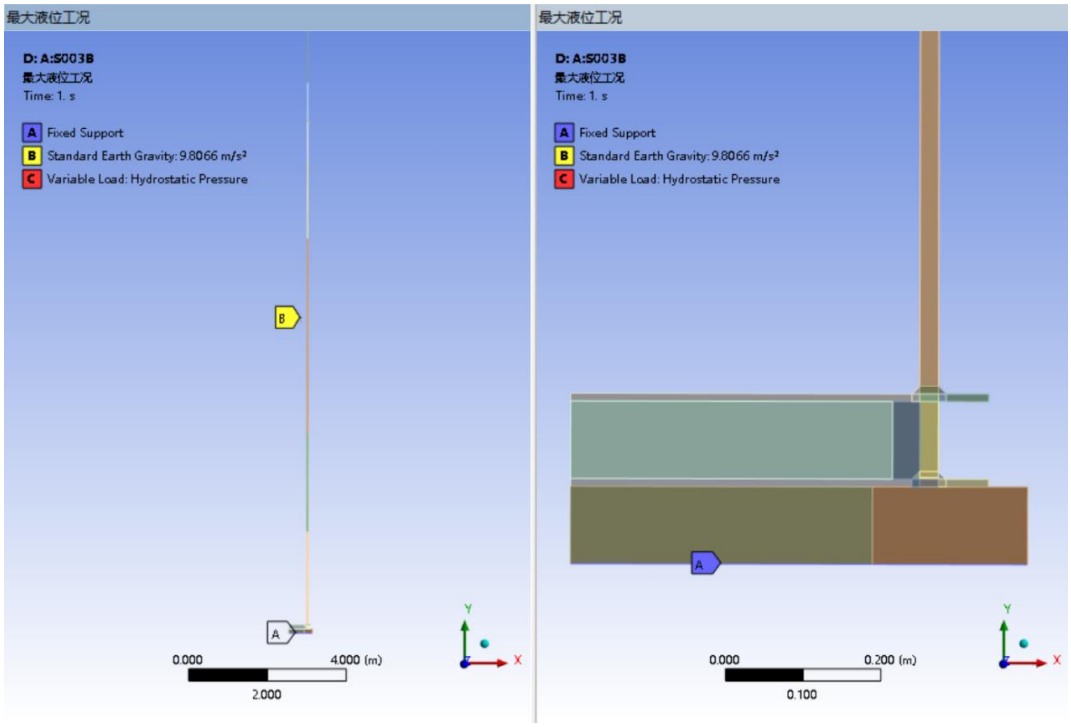

Figure 9. Hydrostatic loading scheme applied to the tank wall and bottom, simulating full-capacity liquid storage under standard gravity (9.8 m/s²)

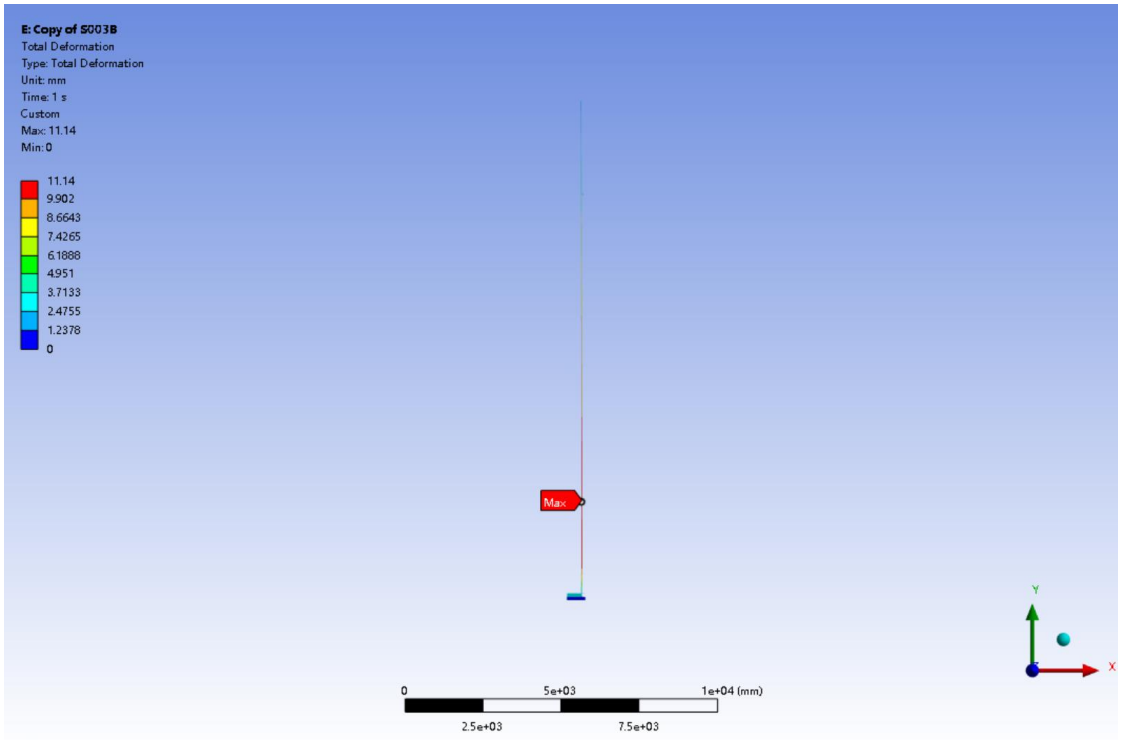

Figure 10. Deformation contour of Structure A under hydrostatic loading

Loading: Hydrostatic pressure is applied vertically to the tank bottom and shell, corresponding to fluid height and a gravity acceleration of 9.8 m/s². Self-weight is also included in the simulation.

3. Structural response analysis under hydrostatic loading

Finite element simulations are conducted under uniform hydrostatic loading to evaluate the mechanical performance of five double-layer tank bottom configurations. Key response metrics—maximum vertical deformation, peak von Mises stress, and their spatial distributions—are extracted to identify structural vulnerabilities and assess support effectiveness in stress reduction and deformation control.

Hydrostatic pressure is applied to the inner surfaces of the tank bottom and shell, simulating a fully filled tank under gravity (9.8 m/s²). The detailed loading scheme is shown in Fig. 9.

3.1 Stress and deformation analysis of structure A

Structure A features an external second bottom plate filled with sand and a concrete ring beam, without any elastic support layer. As shown in Fig. 10, the maximum vertical deformation reaches 11.14 mm, occurring at the upper section of the second shell course.The peak von Mises stress is 434.39 MPa, concentrated at the fillet weld connecting the second bottom plate to the tank wall (Fig. 11).

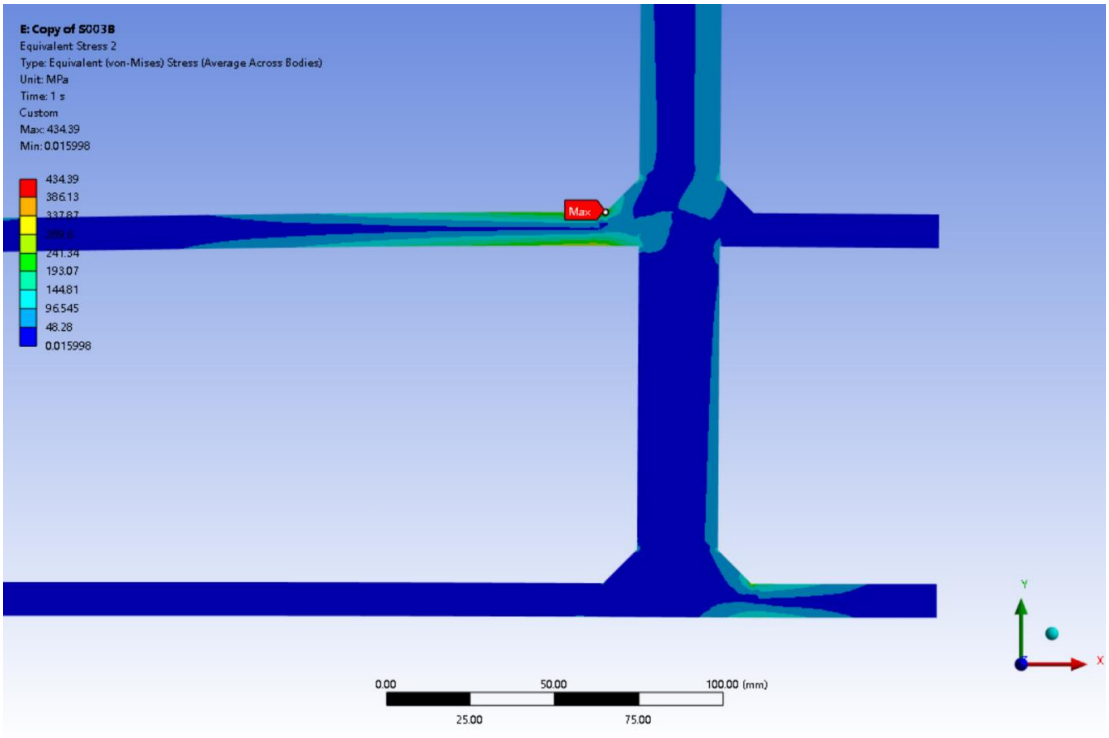

Figure 11. Stress distribution of Structure A, showing localized concentration at the weld joint

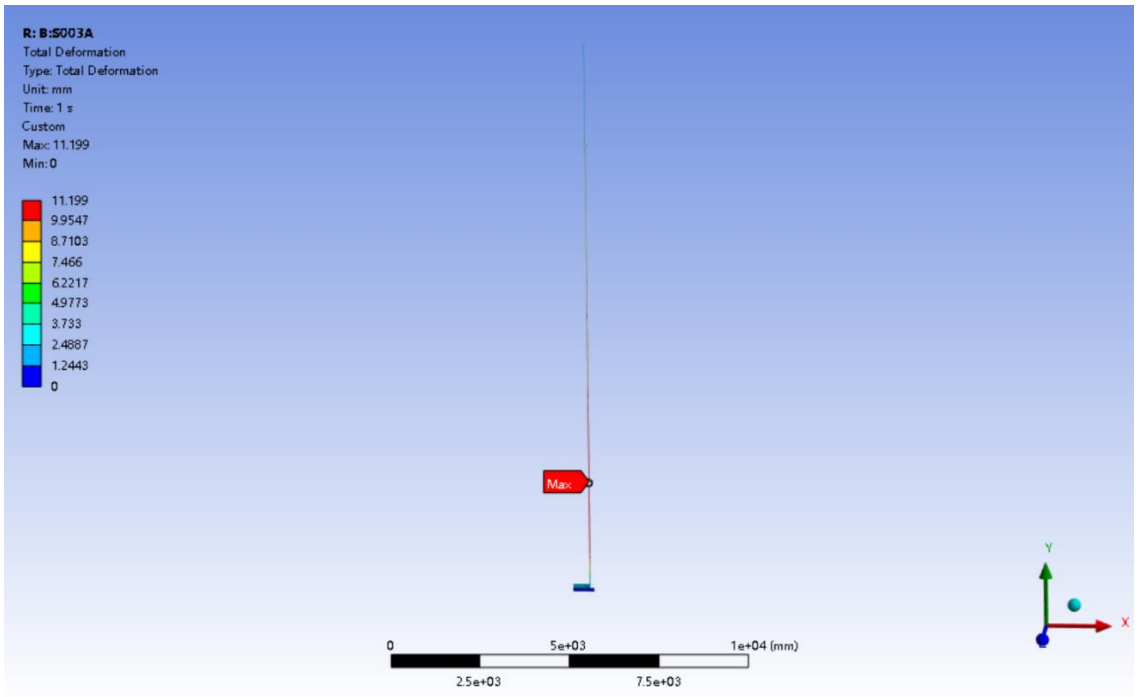

Figure. 12 Deformation contour of Structure B with elastic foundation

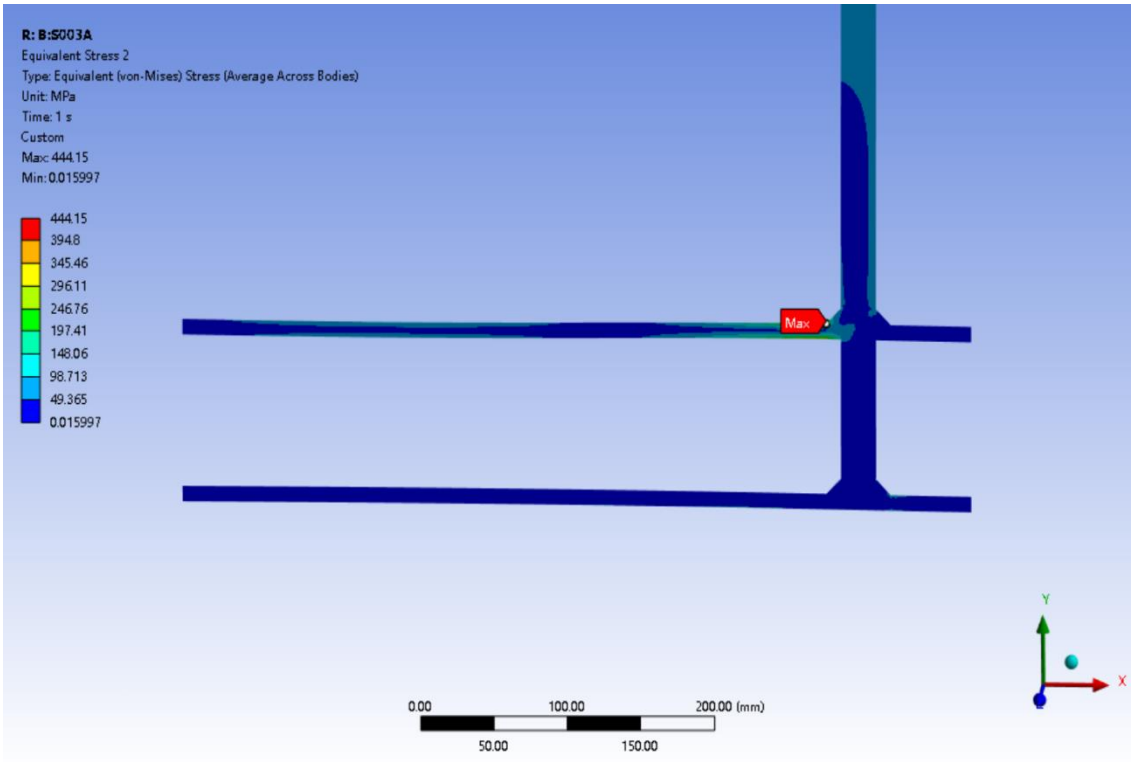

Figure 13. Stress contour of Structure B showing stress intensification near the weld

These results indicate a pronounced local stress concentration due to the absence of a compliant base, which limits the structure's ability to redistribute stress effectively under fluid loading.

3.2 Stress and deformation analysis of structure B

Structure B is a variation of Structure A, with an added elastomeric rubber cushion beneath the base to simulate a flexible foundation.The maximum deformation slightly increases to 11.20 mm (Fig. 12), with the deformation zone remaining at the second shell course. The peak stress rises marginally to 444.15 MPa, again concentrated at the weld region (Fig. 13).

The expected stress mitigation effect from the rubber pad is not observed; on the contrary, the increased flexibility appears to transfer additional deformation to the weld region, exacerbating local stress.

3.3 Stress and deformation analysis of structure C

Structure C incorporates an internal second bottom plate supported by intermediate steel pads positioned between the upper and lower layers.

The maximum vertical deformation remains at 11.14 mm (see Fig. 14), which is comparable to that observed in Structures A and B.

However, the peak von Mises stress is significantly reduced to 305.08 MPa, while still occurring

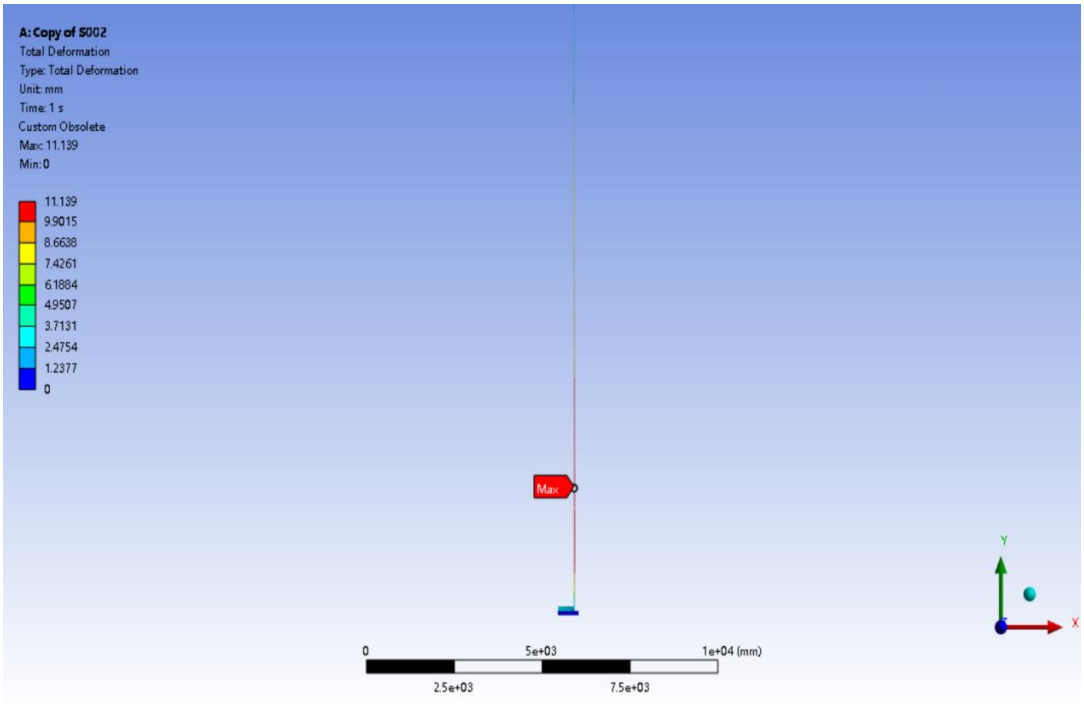

Figure 14. Deformation distribution of Structure C with internal support pads

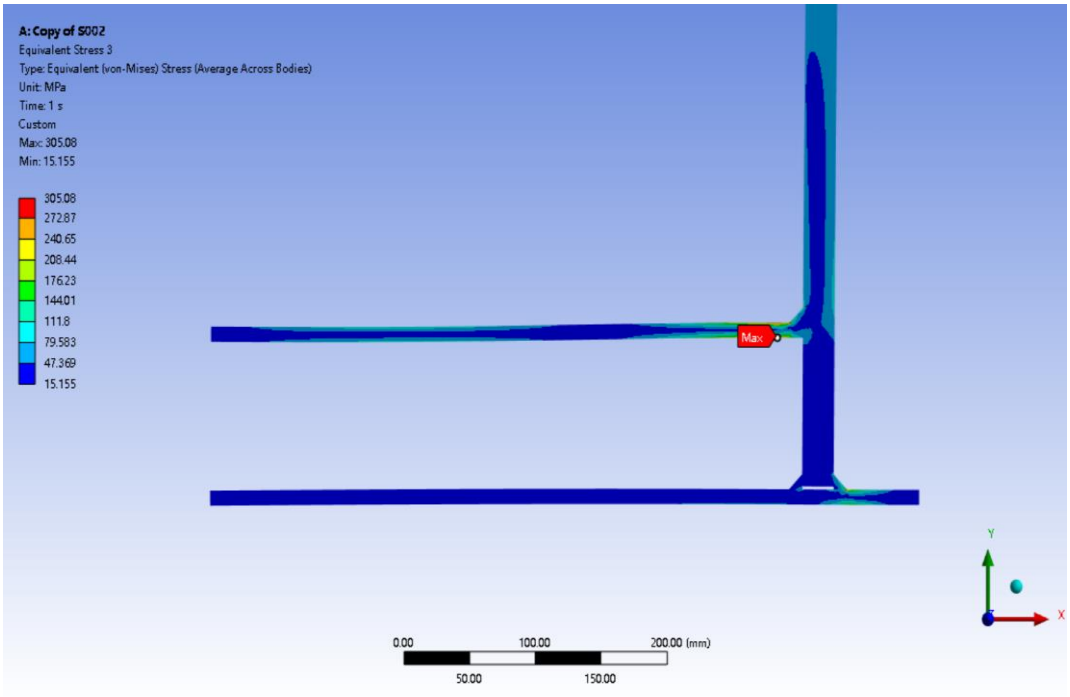

Figure 15. Stress field of Structure C, illustrating improved stress redistribution

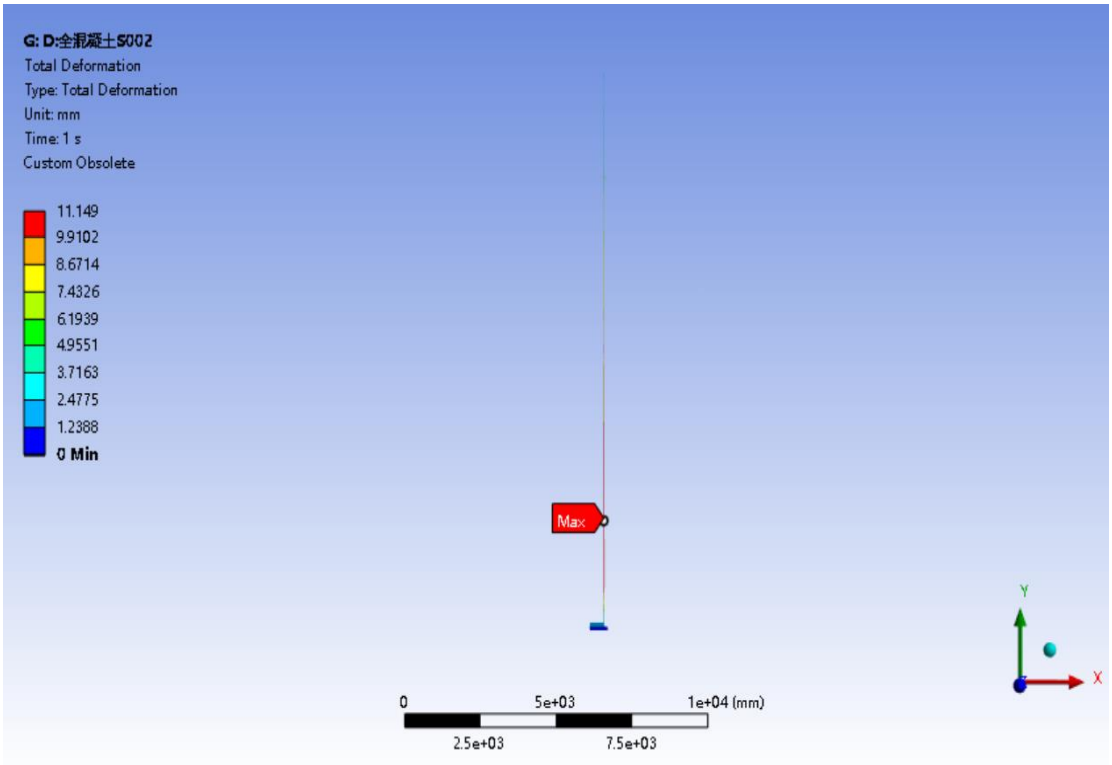

Figure 16. Deformation contour of Structure D with fully filled concrete

at the fillet weld between the bottom plate and tank wall (Fig. 15). This demonstrates that the addition of internal support elements effectively mitigates localized stress concentration without increasing global deformation, thereby improving the overall mechanical performance of the structure.

The internal supports help distribute vertical loads more uniformly across the bottom surface, thereby reducing the severity of localized stress at critical connections.

3.4 Stress and deformation analysis of structure D

Structure D builds upon Structure C by fully filling the interlayer with concrete, providing continuous contact and increased stiffness.The maximum vertical deformation is 11.15 mm (Fig. 16), nearly unchanged from previous cases.The peak von Mises stress further decreases to 245.87 MPa (Fig. 17), indicating an effective reduction of stress concentration.

The concrete filler substantially enhances compressive rigidity and helps homogenize the stress field. Structure D demonstrates the most favorable performance among the 2D configurations in terms of stress control and stiffness.

3.5 Stress and deformation analysis of structure E

Structure E adopts a three-dimensional I-beam steel support grid beneath the tank bottom,

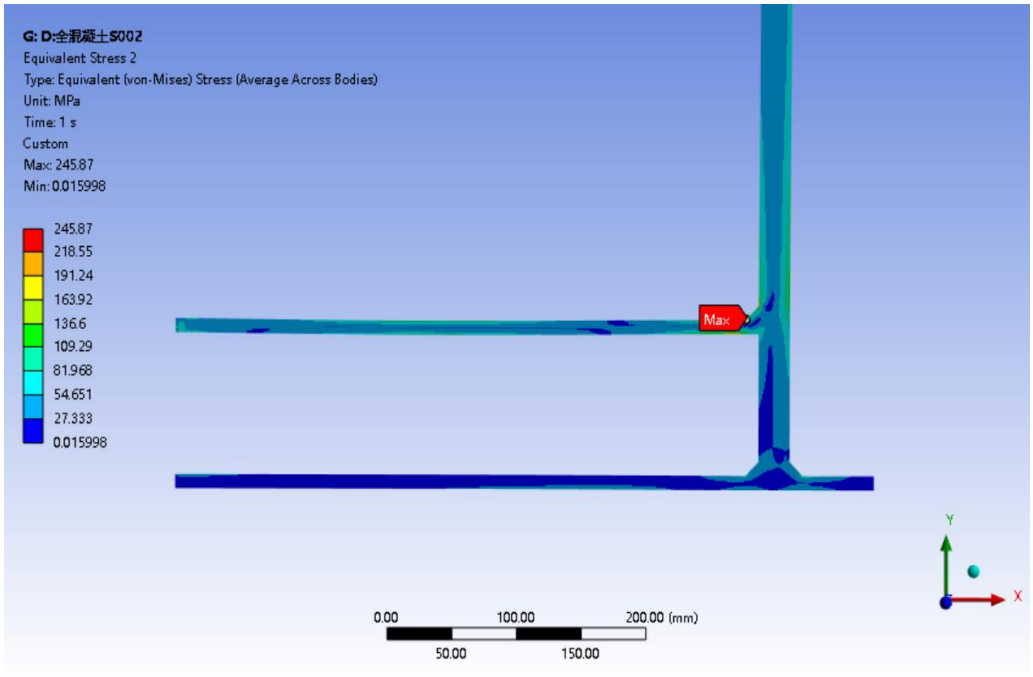

Figure 17. Stress contour of Structure D, showing a uniform and low-stress profile

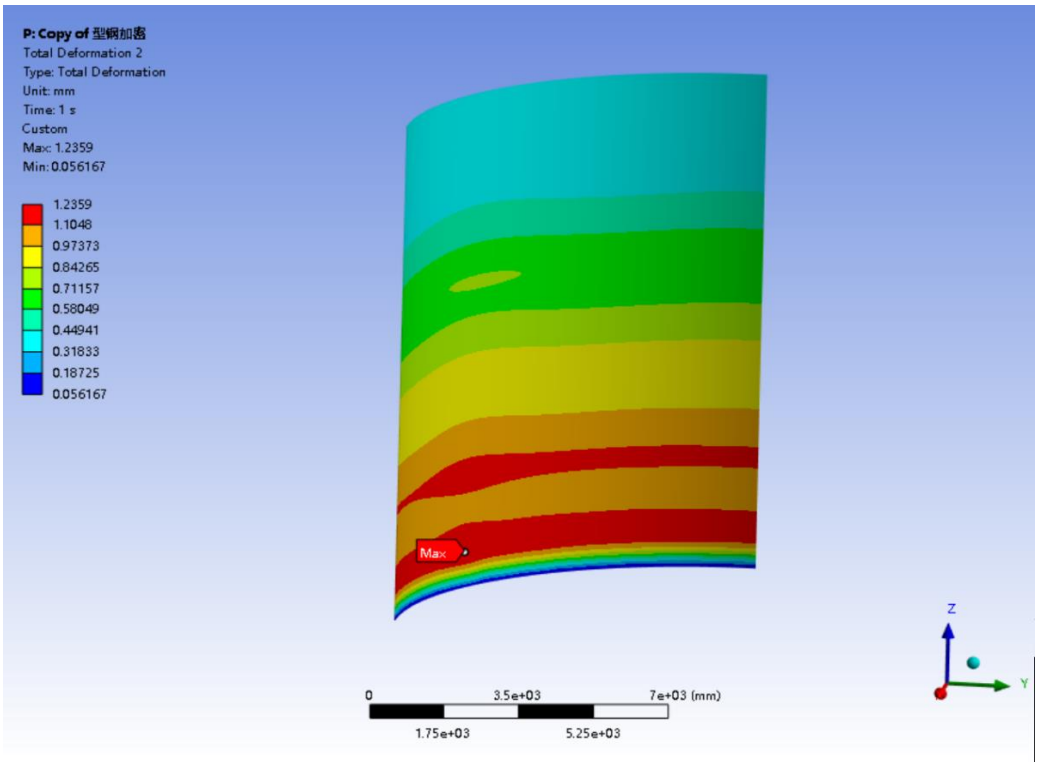

Figure 18. Wall deformation of Structure E under hydrostatic pressure

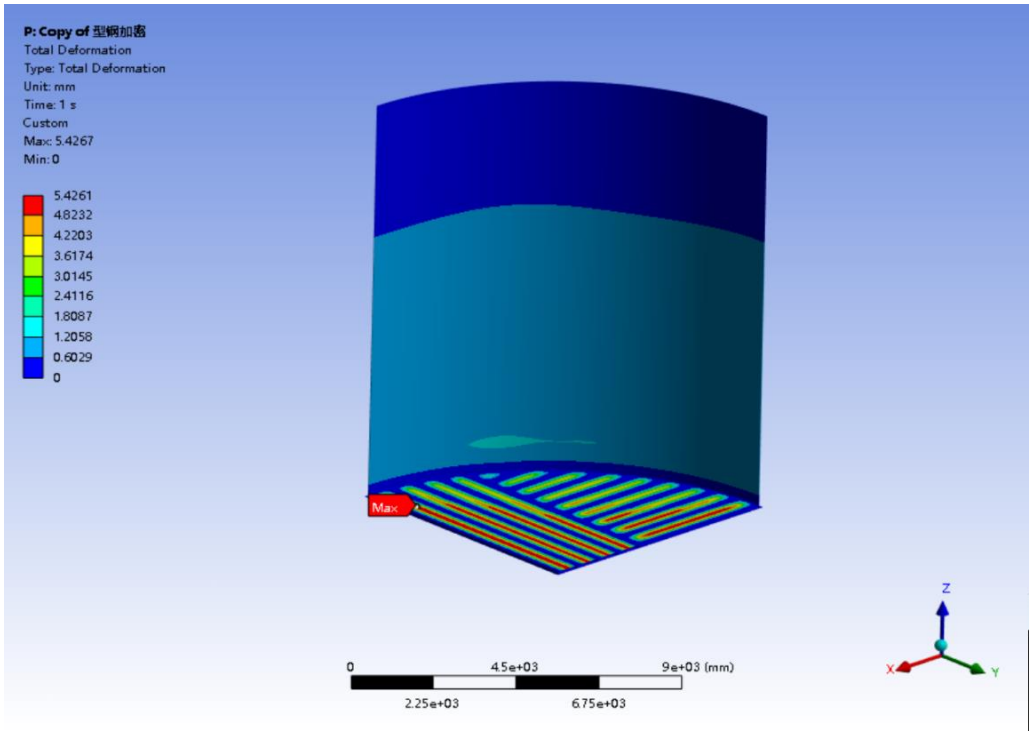

Figure 19. Total deformation contour of Structure E

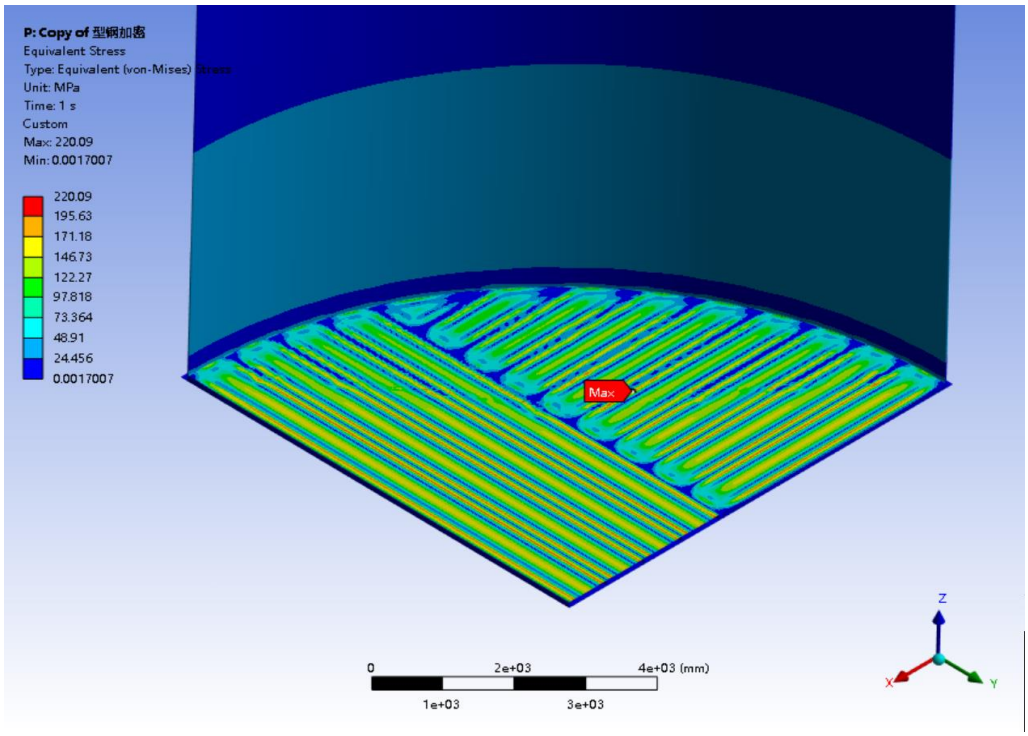

Figure 20. Stress field of Structure E, with low-intensity concentration near support interfaces

Table 3. Summary of mechanical performance and observations for each tank bottom structure

Structure	Max Deformation (mm)	Max von Mises Stress (MPa)	Key Observations
A	11.14	434.39	Severe stress at weld, no elastic base
B	11.20	444.15	Slight increase in stress with rubber pad
C	11.14	305.08	Internal supports reduce stress effectively
D	11.15	245.87	Best uniformity and stiffness among 2D designs
E	5.42 (overall)	220.00	Optimal performance; high complexity

providing enhanced spatial stiffness distribution and localized load resistance.

As a result, the maximum deformation of the tank wall is significantly reduced to 1.2 mm (Fig. 18), while the overall structural deformation is limited to 5.42 mm (Fig. 19), representing the smallest displacement among all configurations analyzed.

The peak von Mises stress is correspondingly reduced to 220.00 MPa, located at the interface between the bottom plate and the steel I-beam support (Fig. 20). This indicates that the integration of a rigid support framework is effective in both stress attenuation and deformation control, particularly for applications requiring high structural rigidity and minimal displacement.

The high structural stiffness provided by the steel frame effectively suppresses both vertical deformation and localized stress. However, the complexity of the I-beam layout increases design and construction demands, making it more suitable for critical or high-reliability applications.

3.6 Summary and selection of reference structure

The simulation results of the five structural configurations are summarized in Table 3, highlighting key mechanical performance indicators and design observations.

Among all designs, Structure D demonstrates the most balanced performance, featuring significantly improved stress control, uniform stress distribution, and moderate deformation, while maintaining a reasonable design complexity. Accordingly, Structure D is selected as the reference configuration for the subsequent parametric investigations in Chapter 4, which examine the influence of rubber pad thickness and stiffness on structural response.

4. Influence of rubber pad parameters

To further investigate the influence of support interface characteristics on the mechanical performance of double-layer tank bottom structures, Structure D—which exhibited superior stress distribution and deformation control in prior analyses—is selected as the reference model for this parametric study.

The objective is to assess how variations in rubber pad parameters, specifically thickness and elastic modulus, impact critical structural response indicators, namely the maximum von Mises stress and maximum vertical deformation.

All simulations are conducted under uniform hydrostatic loading conditions to ensure methodological consistency and enable objective comparison across different parametric configurations.

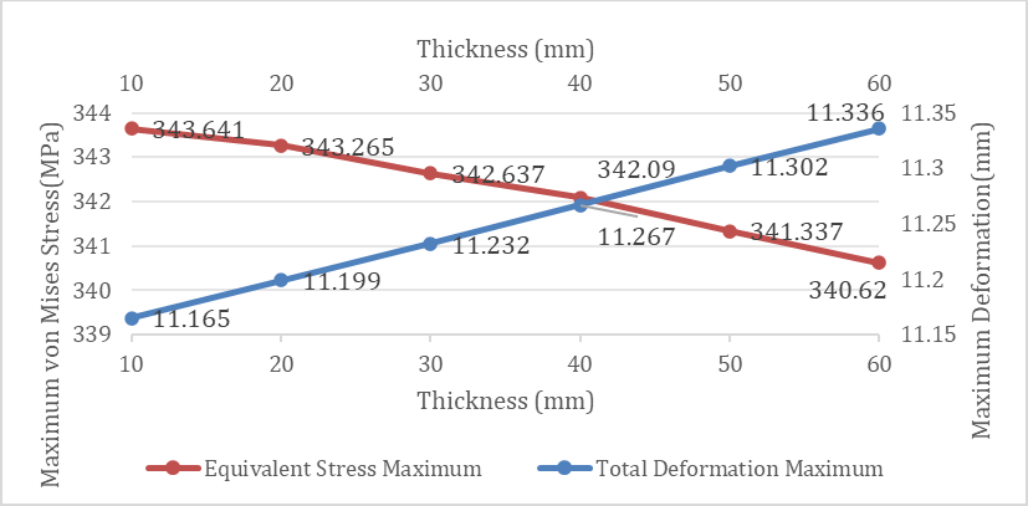

Figure 21. Influence of rubber pad thickness on structural response of Structure D: variations in maximum von Mises stress and vertical deformation under hydrostatic loading

4.1 Effect of rubber pad thickness on structural response

In this subsection, the elastic modulus of the rubber pad is held constant at 5.7 MPa, corresponding to the mechanical properties of EPDM rubber, while the pad thickness is varied across five levels: 10 mm, 20 mm, 30 mm, 40 mm, and 50 mm.

The results of the finite element simulations are presented in Fig. 21, which illustrates the relationship between pad thickness and the two key structural response metrics: maximum von Mises stress and maximum vertical deformation.

The simulation results reveal the following trends:

a) The maximum vertical deformation exhibits a modest upward trend, increasing from 11.05 mm at a pad thickness of 10 mm to 11.22 mm at 50 mm, corresponding to an absolute increase of 0.17 mm, or approximately 1.5%.

b) The maximum von Mises stress shows a marginal decrease, declining from 246.13 MPa to 242.91 MPa, representing a 1.3% reduction.

These results indicate that increasing rubber pad thickness has a limited but quantifiable influence on structural response. While greater thickness enables increased compressibility and minor energy absorption, which slightly reduces local stress levels, it also results in slightly increased global deformation. Overall, the effect of pad thickness variation on global stiffness and stress mitigation remains minimal within the tested range.

Accordingly, in practical engineering applications, the selection of rubber pad thickness should be guided primarily by considerations such as construction tolerance, installation space constraints, or vibration damping requirements, rather than by its marginal impact on the structure's load-bearing capacity.

4.2 Effect of rubber pad elastic modulus on structural response

In this subsection, the effect of rubber pad stiffness on the mechanical response of the tank

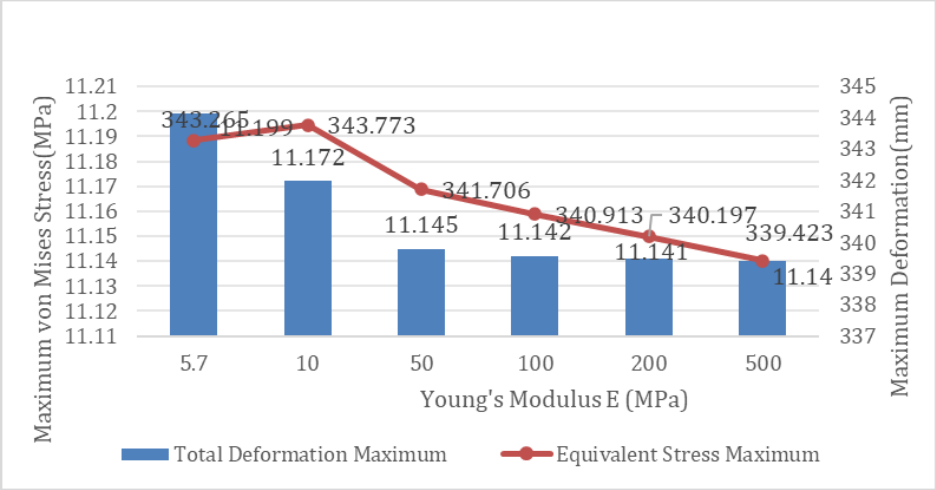

Figure 22. Effect of rubber pad elastic modulus on maximum stress and vertical deformation of Structure D under hydrostatic loading

bottom structure is examined by varying the elastic modulus (E) of the pad material. The thickness of the rubber pad is held constant at 20 mm, while the elastic modulus is varied across five representative values—2 MPa, 5 MPa, 10 MPa, 15 MPa, and 20 MPa—to reflect the typical stiffness range of commonly used elastomeric materials.

For each modulus configuration, the corresponding maximum vertical deformation and maximum von Mises stress are extracted from the finite element simulations. The results are presented in Fig. 22, which illustrates the relationship between rubber stiffness and structural response under hydrostatic loading. This trend suggests the presence of diminishing returns—beyond a certain stiffness threshold, further increases in modulus yield only marginal structural benefit. This observation is consistent with findings from modified Mooney–Rivlin modeling approaches used in nonlinear rubber analysis under constraint conditions [20].

Analysis results and interpretation

Simulation results show that as the elastic modulus increases from 2 MPa to 20 MPa, both peak von Mises stress and maximum vertical deformation decrease slightly—from 248.4 MPa to 244.3 MPa (≈1.6%) and from 11.17 mm to 11.11 mm (≈0.54%), respectively.

This indicates a moderate stabilizing effect, where increased stiffness marginally reduces stress concentration and displacement. The trend aligns with prior studies [21], which suggest diminishing returns beyond a certain stiffness threshold.

Although elastic modulus is a relevant design parameter, its influence on global performance is limited compared to factors like plate configuration and support layout. In practice, moderate-stiffness elastomers (e.g., polyurethane with E ≈ 10–50 MPa) provide an effective balance between cushioning and load-bearing, without the need for high-modulus materials.

Combined Conclusions on Thickness and Modulus Effects

Based on the parametric analyses in Sections 4.1 and 4.2, the following conclusions are drawn:

(a) Rubber pad thickness and elastic modulus both influence mechanical response, but their effects are secondary to global structural factors.

Table 4. Correlation between rubber pad elastic modulus and representative engineering materials

Elastic Modulus E (MPa)	Representative Material Types	Engineering Application Description
5–7	EPDM, Styrene-Butadiene Rubber (SBR)	Soft cushioning materials for vibration isolation and moderate deformation zones
10	High-hardness rubber, Natural rubber, Polyurethane foam	Moderately elastic materials for compressive buffering and soft support layers
50	Semi-rigid Polyurethane, Thermoplastic Elastomers (TPE)	Suitable for low-structural-load support pads and semi-stiff foundation cushions
100	Rigid Polyurethane, Nylon blocks	Used for rigid support with limited deformation tolerance
200	Engineering Plastics (e.g., Polyamide, PA)	High-stiffness components for anti-deformation applications

(b) Pad thickness mainly affects vertical deformation, with minimal impact on stress.

(c) Elastic modulus influences both stress and deformation, though improvements from increased stiffness are modest.

(d) Therefore, rubber pad parameters can be flexibly optimized—particularly within the 10–50 MPa range—to meet project-specific needs such as settlement, vibration, or material availability.

(e) These results provide a basis for material selection, as elaborated in Section 4.3, and support the application of multiphysics elastomer optimization strategies [22], especially where both deformation and stress must be managed.

4.3 Correlation between elastic modulus and material types

Effective material selection for support layers must consider not only mechanical performance (e.g., stress and deformation) but also inherent properties, availability, and application relevance. To bridge simulation results with practical design, representative material types were mapped to elastic modulus ranges based on relevant standards, databases, and literature, as summarized in Table 4.

This mapping offers a practical reference framework for selecting rubber pad or polymer-based support materials in accordance with design requirements for stiffness, deformability, and long-term durability.

It further underscores that materials with an elastic modulus in the range of 10–50 MPa—such as polyurethane and thermoplastic elastomers (TPEs)—achieve an optimal balance between structural support and flexibility, making them especially suitable for double-layer tank bottom applications that demand moderate stress attenuation and geometric adaptability.

Engineering Implication

Although previous simulations have demonstrated that rubber pad stiffness and thickness exert only minor influence on global structural behavior, their contribution to stress redistribution, localized deformation control, and construction interface compatibility remains non-negligible. Accordingly, material selection should follow a multi-criteria decision-making approach, considering the following aspects:

(1) Mechanical performance as derived from finite element simulations

(2) Material stiffness characteristics and formability under practical loads

(3) Cost-effectiveness and market availability of candidate materials
(4) Ease of construction and installation, especially in constrained foundation environments

This comprehensive material–property correlation serves as the analytical foundation for the cost–performance evaluation model introduced in Section 4.4, which further refines material selection recommendations for engineering implementation.

4.4 Material comparison and cost–performance analysis recommendations

To enhance the practical value of the simulation results, this study establishes a cost–performance framework linking elastic modulus with representative engineering materials, including EPDM, SBR, natural rubber, polyurethane, nylon, and HDPE. This integrative approach reflects actual engineering decision-making and supports rational material selection based on mechanical functionality and economic feasibility, as also demonstrated in hybrid material optimization studies [20].

Candidate materials for rubber pads in double-layer tank bottoms exhibit varying stiffness-performance profiles. Low-modulus materials (5–10 MPa), such as EPDM and SBR, are highly deformable and cost-effective, suitable for settlement buffering and non-critical zones, though limited in load-bearing capacity. Medium-modulus materials (10–50 MPa), including natural rubber, polyurethane, and thermoplastic elastomers (TPEs), offer a favorable balance between stiffness and compliance. These materials effectively reduce local stress concentrations while accommodating moderate deformation, making them broadly applicable in foundation supports, pipelines, and seismic joints. High-modulus materials (100–500 MPa), such as HDPE, engineering plastics (PA6, PA66), and composites, provide excellent compressive strength and dimensional stability but lack elasticity and are expensive, thus more appropriate for rigid support components under stringent performance requirements.

Among these, medium-modulus elastomers represent the most technically balanced and cost-effective solution for tank foundation applications, a conclusion reinforced by recent evaluations of hybrid polymer support systems [23].

Recommended material range for engineering applications

To balance structural safety, cost efficiency, and constructability, materials with elastic moduli between 10–50 MPa are recommended. Polyurethane-based and thermoplastic elastomers (TPEs) offer optimal engineering performance, effectively reducing peak von Mises stress and vertical deformation while providing sufficient compliance for settlement and interface irregularities. These materials are also well-suited to both prefabricated and in-situ installation. As such, medium-modulus elastomers present the most practical and cost-effective choice for double-layer tank bottoms requiring moderate stiffness and deformation adaptability. Similar nonlinear behavior has been observed in layered elastomeric systems under operational loads [24].

Data sources and industry validation

The material classifications and performance assessments in this section are substantiated by the following authoritative references: the Manual of Rubber Material and Product Performance Testing [25], the Engineering Plastics Handbook by [26], the European Rubber Journal [34], and the comparative study on structural elastomer behavior and cost performance by Shen et al. [28]. This multi-source triangulation enhances the credibility of the modulus–material mapping and provides a robust empirical foundation for practical engineering applications.

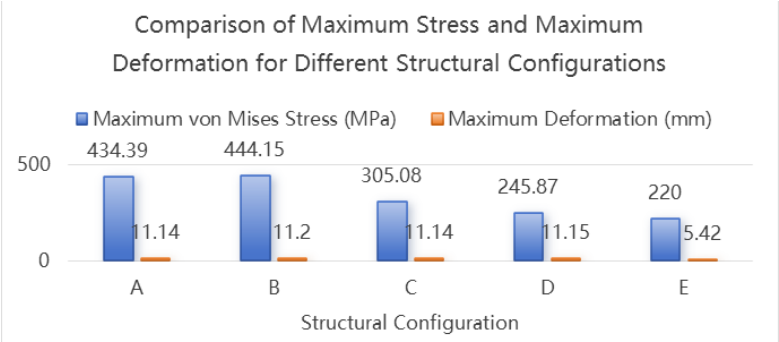

Figure 23. Comparison of maximum stress and vertical deformation across Structures A to E under hydrostatic loading

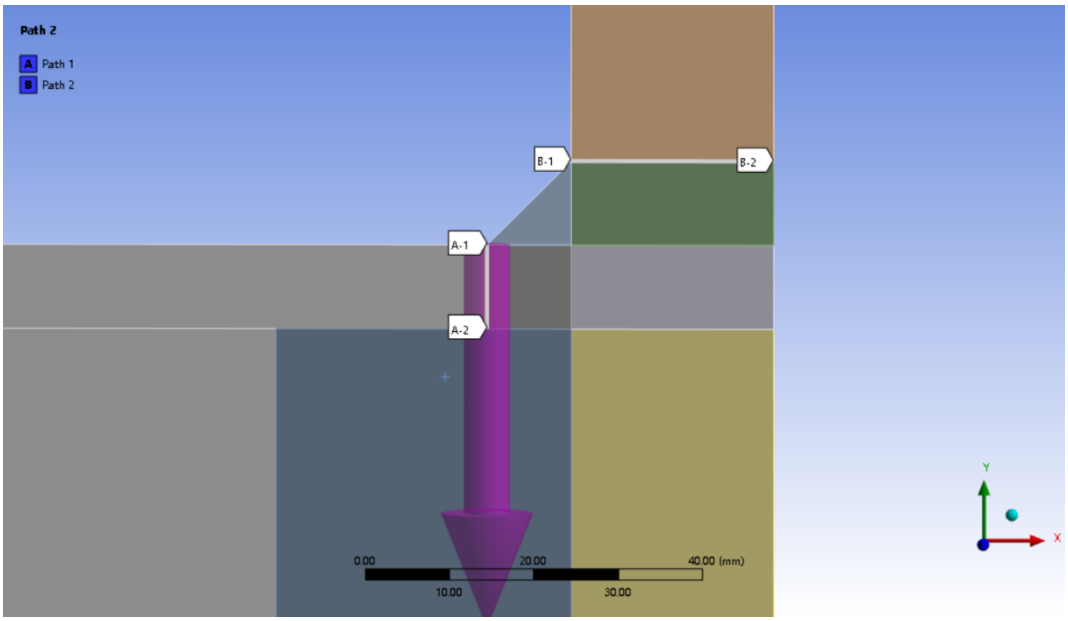

Figure 24. Definition of linearized stress evaluation paths: Path 1 (bottom fillet weld), Path 2 (shell interface)

5. Structural performance comparison and optimization evaluation

5.1 Global stress and deformation comparison

Fig. 23 summarizes the maximum von Mises stress and total vertical deformation for each structural configuration.

Simulation results show that Structures A and B exhibit high stress concentrations exceeding 430 MPa, primarily at the fillet welds between the second bottom plate and tank wall, with deformations around 11.14-11.20 mm. Structures C and D perform better due to internal supports and concrete fill, with Structure D offering the most uniform stress distribution. Structure E, featuring a 3D steel support grid, achieves the lowest stress and minimal deformation (5.42 mm),

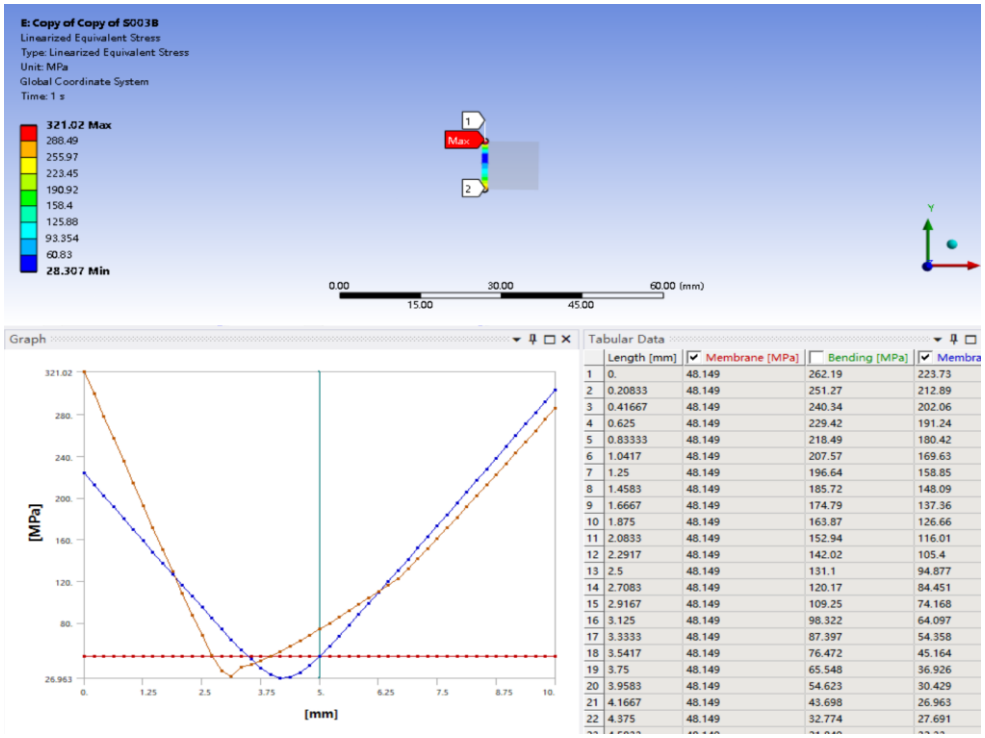

Fig. 25 Linearized stress profile along Path 1 for Structure A.

though its structural complexity limits its use to high-reliability applications requiring stringent stiffness control.

5.2 Linearized stress distribution analysis

To assess localized stress behavior, two stress classification paths are defined (Fig. 24). Path 1 follows the fillet weld between the second bottom plate and tank wall to capture stress at the horizontal-vertical transition; Path 2 runs vertically along the first-course shell plate to reflect stress gradients in the wall. These paths support linearized stress decomposition into membrane and bending components, following GB/T 4732 (Ministry of Housing and Urban-Rural Development of PRC, 2010), enabling systematic comparison of local stress responses across structural configurations.

As an example, Fig. 25 presents the linearized stress distribution along Path 1 for Structure A, showing the membrane stress, bending stress, and their algebraic sum. The peak stress value is also indicated for comparison.

According to GB/T 4732, the following criteria are applied for evaluating stress acceptability:

- Membrane stress limit: 1.5 × allowable stress = 180 MPa
- Membrane + bending stress limit: 3 × allowable stress = 360 MPa

The linearized stress classification results for all configurations along the two paths are summarized in Tables 5, 6, respectively.

All evaluated structures satisfy the allowable limits defined by the GB/T 4732 standard,

indicating compliance with safety requirements under the prescribed hydrostatic loading conditions. However, the available safety margins vary notably among configurations. Structure D demonstrates the most favorable performance, maintaining the lowest combined stresses and peak values, while Structures A and B exhibit stress magnitudes approaching design limits, indicating reduced structural robustness.

5.3 Optimization recommendations

Comprehensive evaluation of deformation and stress distribution yields the following recommendations [29]:

Structure D offers the most balanced performance, with minimal peak stress, uniform stress fields, and adequate stiffness. Its configuration is consistent with the multilayer optimization strategies proposed by [20] and is recommended as the baseline design for general-purpose applications.

Structure C achieves effective stress reduction with reduced construction complexity by omitting full concrete infill. It is suitable for projects constrained by cost or constructability.

Structure E, supported by a steel I-beam grid, shows superior stiffness and minimal deformation. Validated hybrid-support strategies and elastomeric damping benefits [27, 33, 35] make it ideal for seismic or high-reliability applications, despite its fabrication complexity.

Structures A and B exhibit high stress concentrations at welds, with peak values near or above yield strength. Due to limited fatigue resistance, they are not recommended for high-pressure or long-term loading environments.

5.4 Design guidance summary

This comparative study provides quantitative support for selecting structural layouts and support materials in double-layer tank bottoms. Key insights include:

Structure D, with internal supports and full concrete infill, delivers optimal performance in stress control and constructability, making it the preferred solution for most applications.

Elastic pads (e.g., in Structure B) do not guarantee stress reduction unless their stiffness is well-matched to the overall structure, underscoring the need for material-structure compatibility.

Effective stress mitigation requires co-optimization of material properties and geometric design; isolated adjustments (e.g., increasing pad thickness) offer limited benefits without system-level integration.

These findings form the basis for the comprehensive recommendations in Chapter 6.

6. Conclusions

This study establishes a multi-parameter evaluation framework for optimizing double-layer tank bottom systems through finite element analysis and sensitivity studies. Key conclusions are as follows:

Structure D, featuring full concrete infill beneath the second bottom plate, delivers optimal performance with minimal von Mises stress, uniform stress distribution, and superior stability. It is recommended for high-reliability storage applications.

Structure E, supported by a steel I-beam grid, offers the highest stiffness and least deformation

but involves complex fabrication, making it suitable only for stiffness-critical or seismically sensitive projects.

Structures A and B exhibit significant stress concentrations near weld joints, with peak stresses approaching yield limits, and are thus unsuitable for high-load or long-term service.

Structure C, incorporating partial internal support pads, provides a balance between stress mitigation and construction simplicity, making it a viable compromise where full concrete filling is impractical.

Rubber pad parameters (thickness, modulus) have limited impact on global response and can be flexibly tuned to meet specific engineering needs such as settlement tolerance, cost control, or damping.

Among candidate materials, polyurethane-based elastomers and TPEs with elastic moduli in the 10–50 MPa range are identified as the most suitable, offering an optimal balance between mechanical performance, deformation compliance, and economic feasibility.

Future work will focus on incorporating soil–structure interaction, fatigue behavior, and material aging effects to enhance the reliability of double-layer tank bottom designs.

Acknowledgments

The authors would like to express their sincere gratitude to Advanced in Computational Design for providing a high-quality academic platform for the dissemination of engineering research. The constructive comments and suggestions from the editorial team and anonymous reviewers are highly appreciated and have contributed significantly to the improvement of this manuscript.

References

1. API (2020). Welded tanks for oil storage (API Standard 650). American Petroleum Institute, Washington, D.C., USA.
2. CEN (2004). Specification for the design and manufacture of site built, vertical, cylindrical, flat-bottomed steel tanks for the storage of liquids at ambient temperature and above (EN 14015). European Committee for Standardization, Brussels, Belgium.
3. Jiao, Y.Q., Zhao, H.D., Zhang, Z.Y., et al. (2023). Analysis of settlement characteristics of large-scale oil tanks considering interaction between foundation and tank body. Chemical Machinery, 50(4), 471-476.
4. Wang, Y., Ma, D., Ren, D.M. (2016). Finite element analysis of metal interface bonding strength and its influencing factors. Mechanical Engineering and Automation, 2016(03), 112-114.
5. Liu, Z.M., Wu, G.F., Gao, Y.F. (2022). Stress analysis and life prediction of storage tank bottom plates considering corrosion. Chemical Equipment and Pipeline, 59(1), 38-42.
6. Sathyanarayanan, H., Adluri, S. (2015). Fatigue stress evaluation at shell-to-bottom joint in tanks under elevated temperature. ASME Journal of Pressure Vessel Technology, 137(4), 041408. https://doi.org/10.1115/1.4029143
7. Santhosh, P., Sharma, M. (2023). Design and simulation analysis of double bottom tank with composite layer using ANSYS. Journal of Material Science Research and Reviews, 17(3), 15-22.
8. Ohsaki, M., Nakamura, H., Tsuda, M. (2015). Finite-element analysis of laminated rubber bearing of building frame under seismic excitation. Earthquake Engineering & Structural Dynamics, 44(6), 853-870. https://doi.org/10.1002/eqe.2489
9. Lai, L., Zhang, Q., Wang, R. (2023). Finite element analysis on strength and durability of spherical laminated elastomeric bearings. Engineering Structures, 298, 115843. https://doi.org/10.1016/j.engstruct.

2023.115843
10. Nguyen, T.V., Tran, M.D., Pham, H.T. (2022). Finite element analysis for three-dimensional hyper-elastic problems. International Journal of Mechanical Sciences, 222, 107192. https://doi.org/10.1016/j.ijmecsci.2022.107192
11. Meghashree, R., Patil, M.B., Hiremath, S. (2025). Elastomeric bearing performance prediction using finite element and machine learning techniques. Structures, 55, 937-949. https://doi.org/10.1016/j.istruc.2023.04.021
12. Zhang, Y., Liu, X., Zhou, W. (2023). Digital twin-based monitoring and failure prediction for large oil storage tanks. Engineering Structures, 278, 115372. https://doi.org/10.1016/j.engstruct.2022.115372
13. IRJAES (2017). Numerical modeling of elastomeric bearings using ANSYS. International Research Journal of Advanced Engineering and Science, 2(1), 115-119.
14. Kim, J., Park, C., Lee, H. (2022). Smart monitoring of bottom plate corrosion using embedded sensors in tank foundations. Journal of Pressure Vessel Technology, 144(3), 031402. https://doi.org/10.1115/1.4053385
15. Hoang, T., Fu, Y., Mechitov, K., et al. (2020). Autonomous end-to-end wireless monitoring system for railroad bridges. Advances in Bridge Engineering, 1(1), 17. https://doi.org/10.1186/s43251-020-00014-7
16. Lim, H., Lee, J. (2021). Finite element modeling and experimental validation of rubber bearings for civil infrastructure. Materials and Structures, 54, 39. https://doi.org/10.1617/s11527-021-01627-w
17. Shon, C.S., Estakhri, C.K., Lee, D., Zhang, D. (2016). Evaluating feasibility of modified drilling waste materials in flexible base course construction. Construction and Building Materials, 116, 79-86. https://doi.org/10.1016/j.conbuildmat.2016.04.100
18. Manap, I., Galymzhankyzy, A., Omarova, Z., Ualiyev, D., Temirbekov, D., Shon, C.S., ... Kim, J.R. (2025). Can geopolymer mixture be a solution for utilizing waste glass and basic oxygen furnace slag as aggregates? E3S Web of Conferences, 612, 04001. https://doi.org/10.1051/e3sconf/202561204001
19. Sharipkhan, N., Clifford, O., Perveen, A., Zhang, D., Wei, D.M. (2024). Investigation of co-extrusion using a coat hanger die with different feedblock cross-section. Key Engineering Materials, 973, 131-137. https://doi.org/10.4028/p-RcTKV4
20. Ajan, B., Zhang, D., Spitas, C., Abou Fakhr, E., & Wei, D. (2023). Geometry optimization of a double-layered inertial reactive armor configured with rotating discs. Advances in Computational Design, 8(4), 309-325. https://doi.org/10.12989/acd.2023.8.4.309
21. Kang, H., Lee, S. (2020). Finite element study on rubber-based base isolators under cyclic loading. Advances in Computational Design, 5(2), 127-143. https://doi.org/10.12989/acd.2020.5.2.127
22. Chen, C., Liu, J., Wang, F. (2022). Topology optimization of elastomeric components under multiphysics constraints. Advances in Computational Design, 7(3), 195-209. https://doi.org/10.12989/acd.2022.7.3.195
23. Zhou, H., Zhang, X., Liu, Y. (2023). Performance evaluation of hybrid polymer support systems for storage tank applications. Advances in Computational Design, 8(1), 45-61. https://doi.org/10.12989/acd.2023.8.1.045
24. Igali, D., Perveen, A., Zhang, D., Wei, D. (2020). Shear rate coat-hanger die using Casson viscosity model. Processes, 8(12), 1524. https://doi.org/10.3390/pr8121524
25. Wang, W.Z. (2020). Manual of rubber material and product performance testing. Chemical Industry Press, Beijing, China.
26. Chen, R.S., He, Z.R. (2019). Engineering plastics handbook (2nd Edition). Chemical Industry Press, Beijing, China.
27. Chen, X., Liu, J., Wang, F. (2021). Finite element evaluation of visco-hyperelastic supports in layered composite assemblies. Advances in Computational Design, 6(3), 211-228. https://doi.org/10.12989/acd.2021.6.3.211
28. Shen, W., Zhang, Y., Liu, J. (2021). Mechanical performance and cost evaluation of elastomeric pads in structural joints. Construction and Building Materials, 278, 122321. https://doi.org/10.1016/j.conbuildmat.2020.122321
29. Sharipkhan, N., Perveen, A., Zhang, D., Wei, D.M. (2024). Investigation of the two-channel feedblock

zone in co-extrusion of polymers. Key Engineering Materials, 973, 119-129. https://doi.org/10.4028/p-RN5jhP
30. ANSYS Inc. (n.d.). ANSYS LS-DYNA user's guide-Hyperelastic material definitions. ANSYS Help Online, Canonsburg, USA.
31. ASTM (2014). Standard specification for carbon structural steel, ASTM A36/A36M-14. ASTM International, West Conshohocken, USA.
32. COMSOL Multiphysics (n.d.). Hyperelastic material models. COMSOL Documentation Online, Stockholm, Sweden.
33. Zhang, Y., Wei, D. (2021). Coupled simulation of elastomeric damping in seismic protection for vertical vessels. Advances in Computational Design, 6(2), 159-174. https://doi.org/10.12989/acd.2021.6.2.159
34. European Rubber Journal (2023). Raw material price index reports. Crain Communications, London, UK.
35. Tian, Y., Guo, J., Xie, L. (2021). Numerical analysis of seismic response of large oil tanks considering base isolation systems. Advances in Computational Design, 6(4), 321-336. https://doi.org/10.12989/acd.2021.6.4.321
36. Onopriyenko, Z., Shon, C.S., Zhang, D., Kim, J.R. (2025). Compressive strength and expansion characteristics of BOFS-based geopolymer mortar under different curing regimes. International conference on manufacturing, material and metallurgical engineering, Kuala Lumpur, May.